Origin of the Pseudogap in High-Temperature Cuprate Superconductors

Jamil Tahir-Kheli and William A. Goddard III

Materials and Process Simulation Center (MC 139-74)
California Institute of Technology, Pasadena CA 91125

jamil@wag.caltech.edu, wag@wag.caltech.edu

Supporting Information

Computational details

Calculations to compute the pseudogap (PG) from Equation 1 were performed by averaging 100 ensembles of 2,500 x 2,500 lattices. Four-site plaquettes were randomly doped up to x = 0.187, then three-site plaquettes up to x = 0.226, followed by two-site plaquettes to x = 0.271, and finally one-site plaquettes were doped until no d^9 spins remained at x = 0.317. The details of the doping methodology are described in the manuscript.

The PG was determined for each isolated plaquette along with the average. The average value is the PG observed in bulk measurements (neutron, ARPES, specific heat, etc). STM sees an inhomogenous distribution of PG values. We find the standard deviation of the PG is approximately constant with doping and ~ 15 meV, in agreement with the STM value of ~ 10-20 meV.

Calculations to determine the doping values 0.187, 0.226, 0.271, and 0.317 at the boundaries of plaquette doping of four, three, two, and one undoped Cu d^9 spins were determined by generating a ensemble of 1,000 doped lattices of size 1,000 x 1,000 using a linear scaling percolation algorithm[1].

Details of the ab-initio calculations that lead to out-of-plane hole character

Pure density functionals such as local density (LDA)[2-4] and gradient-corrected functionals (GGA, PBE, etc)[5] obtain a metallic ground state for the undoped cuprates rather than an antiferromagnetic insulator. This is because pure density functionals underestimate the band gap due to a derivative

discontinuity of the energy with respect to the number of electrons.[6,7] In essence, the LDA and PBE functionals include too much self-Coulomb repulsion. This leads to more delocalized electronic states in order to reduce this excess repulsion. Removing this extra repulsion is necessary to obtain the correct localized antiferromagnetic spin states of the undoped cuprates.

This particular problem with LDA has been known for a long time.[8] Very soon after the failure of LDA to obtain the undoped insulating antiferromagnet for cuprates, several approaches were applied to correct the flaws in LDA for La_2CuO_4. Using a self-interaction-corrected method[8] (SIC-LDA), Svane[9] achieved spin localization with an indirect band gap of 1.04 eV, and Temmerman, Szotek, and Winter[10] found a band gap of 2.1 eV. Using an LDA + U method, Czyzyk and Sawatzky[11] obtained 1.65 eV. In all of these calculations on the undoped cuprates, an increase in out-of-plane orbital character was noted in states just below the top of the valence band. Calculations with explicit dopants such as Sr in $La_{2-x}Sr_xCuO_4$ were not done.

Our ab-initio calculations[12,13] were performed using the hybrid density functional, B3LYP. B3LYP has been the workhorse density functional for molecular chemistry computations for almost 20 years due to its remarkable success on molecular systems.[14,15] For example,[14] B3LYP has a mean absolute deviation (MAD) of 0.13 eV, LDA MAD = 3.94 eV, and PBE MAD = 0.74 eV for the heats of formation, ΔH_f, of the 148 molecules in the extended G2 set.[16,17] B3LYP has also been found to predict excellent band gaps for carbon nanotubes and binary and ternary semiconductors relevant to photovoltaics and thermoelectrics.[18,19]

The essential difference between B3LYP and LDA, PBE, and all pure density functionals is that 20% exact Hartree-Fock (HF) exchange is included. B3LYP is called a hybrid functional because it includes exact HF exchange. This removes some of the self-Coulomb repulsion of an electron with itself found in pure DFT functionals. A modern viewpoint of the reason for the success of hybrid functionals is that inclusion of some exact Hartree-Fock exchange compensates the error for fractional charges that occur in LDA, PBE, and other pure density functionals.[20] The downside to using hybrid functionals is they are computationally more expensive than pure density functionals.

Our B3LYP calculations reproduced the experimental 2.0 eV band gap for undoped La_2CuO_4 and also had very good agreement for the antiferromagnetic spin-spin coupling, J_{dd} = 0.18 eV (experiment is ≈ 0.13 eV).[12] We also found substantial out-of-plane apical O and Cu z2 character near the top of the valence band in agreement with LDA + U and SIC-LDA calculations.

We also performed B3LYP calculations on $La_{2-x}Sr_xCuO_4$ for x = 0.125, 0.25, and 0.50 with explicit Sr atoms using large supercells.[13] Regardless of the doping value, we always found that the Sr dopant induces a localized hole in an out-of-the-plane orbital that is delocalized over the four-site region surrounding the Sr as shown in Figure 1 of the manuscript. This is in contrast to removing an electron from the planar Cu x2y2/O pσ as predicted by LDA and PBE.

Our calculations found that the apical O's in the doped CuO_6 octahedron are asymmetric anti-Jahn-Teller distorted. In particular, the O atom between the Cu and Sr is displaced 0.24 Å while the O atom between the Cu and La is displaced 0.10 Å. XAFS measurements[21] find the apical O displacement in the vicinity of a Sr to be ≈ 0.2 Å.

Description of the out-of-plane plaquette orbital obtained from ab-initio QM calculations

Figure 1 of the main text shows the out-of-plane localized hole orbital we obtained in the vicinity of a dopant atom.[12,13,22-24] In $La_{2-x}Sr_xCuO_4$, the formal valence of Sr is +2 and La is +3. This means the environment in the vicinity of Sr is more negatively charged than the average La environment in the crystal. Removing an electron from an out-of-the-plane orbital in the vicinity of the Sr reduces this excess Coulomb repulsion.

Since our calculations had a fixed Néel antiferromagnetic background for the undoped Cu d^9 sites, we found two degenerate states with the plaquette localized as shown in Figures 1(a) and (b). The spin of the plaquette hole state was opposite in the $P_{x'}$ and $P_{y'}$ states due to the fixed Neel antiferromagnetic background (not shown in figure). Exchange coupling of the electron spin of the occupied plaquette state, $P_{x'}$ or $P_{y'}$, makes its spin equal to the spin of the singly occupied x2y2 spin at the Cu site below the apical O p_z.

In our prior work, we assumed that computations with a more realistic background of antiferromagnetic spins would lead to delocalization of the plaquette out-of-plane orbital over all four Cu sites in the plaquette.[12,13,22-24] Thus, including spin, there are four possible out-of-plane plaquette states that are delocalized over a 4-site Cu square. These four states are occupied by three electrons.

The two possible plaquette hole orbital states are shown in figures 1(b) and (c). They have $P_{x'}$ and $P_{y'}$ symmetry and are degenerate in energy if there is only a single dopant in the material and there is no long range antiferromagnetic order in the undoped d^9 region as is found for the superconducting range of dopings. Due to the random dopant environment, the $P_{x'}$ and $P_{y'}$ states can mix to form two orthogonal states with a small energy splitting. The random distribution of these energy splittings in the system is the source of the linear resistivity in our model.[23]

The $P_{x'}$ and $P_{y'}$ out-of-plane plaquettes states above and shown in Figure 1 are different from the delocalized (inside an isolated plaquette) Cu x2y2/O pσ states with the same symmetry, P_x and P_y shown in Figures 3 and S2 (the x2y2/pσ states can be transformed to $P_{x'}$ and $P_{y'}$). It is the latter states that split and lead to the PG. The reason the out-of-plane $P_{x'}$ and $P_{y'}$ energy splitting is not the PG is because they are hole states at ≈ 0.1 eV above the Fermi level as seen in the density of states figures of Perry et al.[13]

Formation of the standard planar Cu x2y2/O pσ band inside the 3D percolating plaquette swath

The Cu x2y2/O pσ states inside 4-site plaquettes are expected to delocalize. The reason for this delocalization is described below.

In models where the O sites are renormalized out, there is a Hubbard on-site Coulomb repulsion, U, and a Cu-Cu hopping matrix element, t_{eff}. In these models, $t_{eff} << U$, leading to localization of spins on the Cu sites.

When the realistic picture that includes the O sites is used, the effective hopping matrix element, t_{eff}, is given by,

$$t_{eff} \sim \frac{t^2}{\left(\varepsilon_d + U - \varepsilon_p\right)}$$

where t is the Cu-O hopping and ε_d and ε_p are the Cu x2y2 and O pσ orbitals energies, respectively. This scenario is shown on the left-side of Figure 1. Localization occurs when $t_{eff} << \varepsilon_d + U - \varepsilon_p$.

The affect of creating a hole in an out-of-plane orbital, as shown in Figure 1, is to lower the orbital energies ε_d and ε_p. Since the largest hole character is on the apical O p_z that resides directly above the Cu atoms and the Cu dz2, the Cu x2y2 orbital energy, ε_d, is lowered much more than the O pσ orbital energy, ε_p. This brings the upper Hubbard Cu orbital energy, $\varepsilon_d + U$, closer to the O orbital, ε_p. The effective hopping matrix element increases and the d^9 spins on the doped Cu sites delocalize. When the plaquettes percolate in 3D through the crystal, the standard Cu x2y2/O pσ band is formed on these doped "four-site" regions (the percolating plaquette swath shown in Figures 2 and S1).

Our explanation for delocalization depends on the detailed differences between the planar Cu and O orbital energies. Renormalizing away the O sites prior to considering the affect of the out-of-plane hole leads to no delocalization because there is no change in the effective hopping, t_{eff}.

Cu x2y2/O pσ delocalization in the plaquettes interacting with localized Cu d^9 spin in the undoped regions leads to explanations for the doping phase diagram, the neutron resonance peak with doping, the dispersionless incommensurabilities found in STM, and the universal room-temperature theromopower[23,24] using simple counting arguments. The first three properties were obtained with no adjustable parameters while the thermopower required exactly one parameter. A large spectrum of additional cuprate phenomenology[22,23] was also qualitatively explained.

Discussion of random placements of plaquettes as a function of doping

Since the dopants minimize their Coulomb repulsion with each other (screened by the percolating metallic electrons), we assume dopants are distributed in the crystal with the constraint of no plaquette overlaps, but otherwise the distribution is completely random. Above ≈ 0.187 doping, it is impossible to add dopants such that the corresponding 4-site plaquette does not overlap (does not share a corner Cu) with a another plaquette. Given that plaquette overlap can no longer be avoided above $x \approx 0.187$, the most energetically favorable location for a dopant to reside is on a site that leads to a 4-site plaquette

doping three Cu d^9 atoms and one doped Cu atom. This is shown as green squares in Figures 2 and S1. At $x \approx 0.226$ doping, it is no longer possible to locate three undoped Cu d^9 sites that are part of a 4-site square. Hence, the most energetically favorable sites are those that dope two Cu d^9 and two doped Cu. These plaquettes are shown in pink in Figures 2 and S1. This form of doping can continue to $x \approx 0.271$. At this point, there are no adjacent pairs of d^9 spin remaining. Single Cu d^9 site doping can continue out to ≈ 0.317. Above this value, there are no remaining localized Cu d^9 spins remaining in the material. The percolating metallic region has become the whole crystal. Figure S1 depicts the undoped d^9 sites and plaquettes as a function of doping for $0.05 < x < 0.32$ and S4 plots the doping evolution of the number of metallic and isolated 4-site plaquettes. At dopings $x \approx 0.05-0.06$, we calculate that the plaquettes percolate in 3D,[1] leading to the formation of the standard Cu x2y2/O pσ metallic band inside the percolating "metallic" swath. Since superconducting pairing occurs at the surface where there are adjacent d^9 spins (green and blue arrows in Figures 2 and S1) and not for isolated spins (pink arrows), superconductivity vanishes at $x \approx 0.271$ in agreement with the experimental value of ≈ 0.27.

Evolution of isolated 4-site plaquettes with doping

Figure S1 (shown on pages 9-11) Schematic of a single CuO_2 plane for twelve different doping values on a 20 x 20 lattice. The dopings span from x = 0.05 to x = 0.32. The black dots are undoped Cu d^9 spins that antiferromagnetically couple to each other. The squares are 4-site plaquettes with Cu atoms at the corners. The out-of-plane orbital and the O atoms are not shown. The black squares are plaquettes that are adjacent (along the Cu-O bond directions) to another plaquette. The red squares are isolated 4-site plaquettes. A delocalized metallic Cu x2y2/O pσ band is formed on the percolating swath of plaquettes for dopings larger than ≈ 0.05. This is shown here in yellow. For dopings less than ≈ 0.151, the percolation occurs in 3D and cannot be seen in this figure. It occurs through coupling of yellow regions to CuO_2 layers above and below the CuO_2 layer that is shown here. Above x = 0.151, 2D percolation occurs and this can be seen directly in the figures. Above 0.187 doping, additional plaquettes must overlap another plaquette. The green squares are 4-site plaquettes that dope three Cu d^9 spins. This occurs from x ≈ 0.187 to x ≈ 0.226. Above 0.226, only two Cu d^9 spins can be doped for each new plaquette. They are shown by pink squares. Above 0.271 doping, only single Cu d^9 spins exist and the blue squares represent the plaquette doping that includes one Cu d^9 spin. There exist undoped adjacent d^9 pairs in the x = 0.26 figure, but in the x = 0.27 figure there are no remaining antiferromagnetic d^9 adjacent pairs to cause superconducting pairing. Thus, the superconducting phase ends at x ≈ 0.271 (experiment is ≈ 0.27). Plaquette doping of a single Cu d^9 (blue squares) can occur up to ≈ 0.317 doping. The final figure at x = 0.32 shows a fully doped crystal with no remaining localized Cu d^9 spins. At this doping, all planar atoms are in the metallic swath. Further doping does not increase the metallic region.

The isolated 4-site plaquettes (red squares) decrease as the doping increases. The density of isolated plaquettes declines sharply at x ≈ 0.19. By x = 0.21 there are no isolated plaquettes in the 20 x 20 lattice here. Isolated plaquettes will always exist in an infinite crystal, but the distance between them becomes so large that they are much farther apart than the neutron spin correlation length, $\xi = a/\sqrt{x}$. This leads

to the PG going to zero at $x \approx 0.19$ as is experimentally observed. This doping value is independent of the magnitude of the isolated plaquette to isolated plaquette coupling (Δ_0 in manuscript). It is a purely geometric consequence of the counting of 4-site plaquettes and their doping.

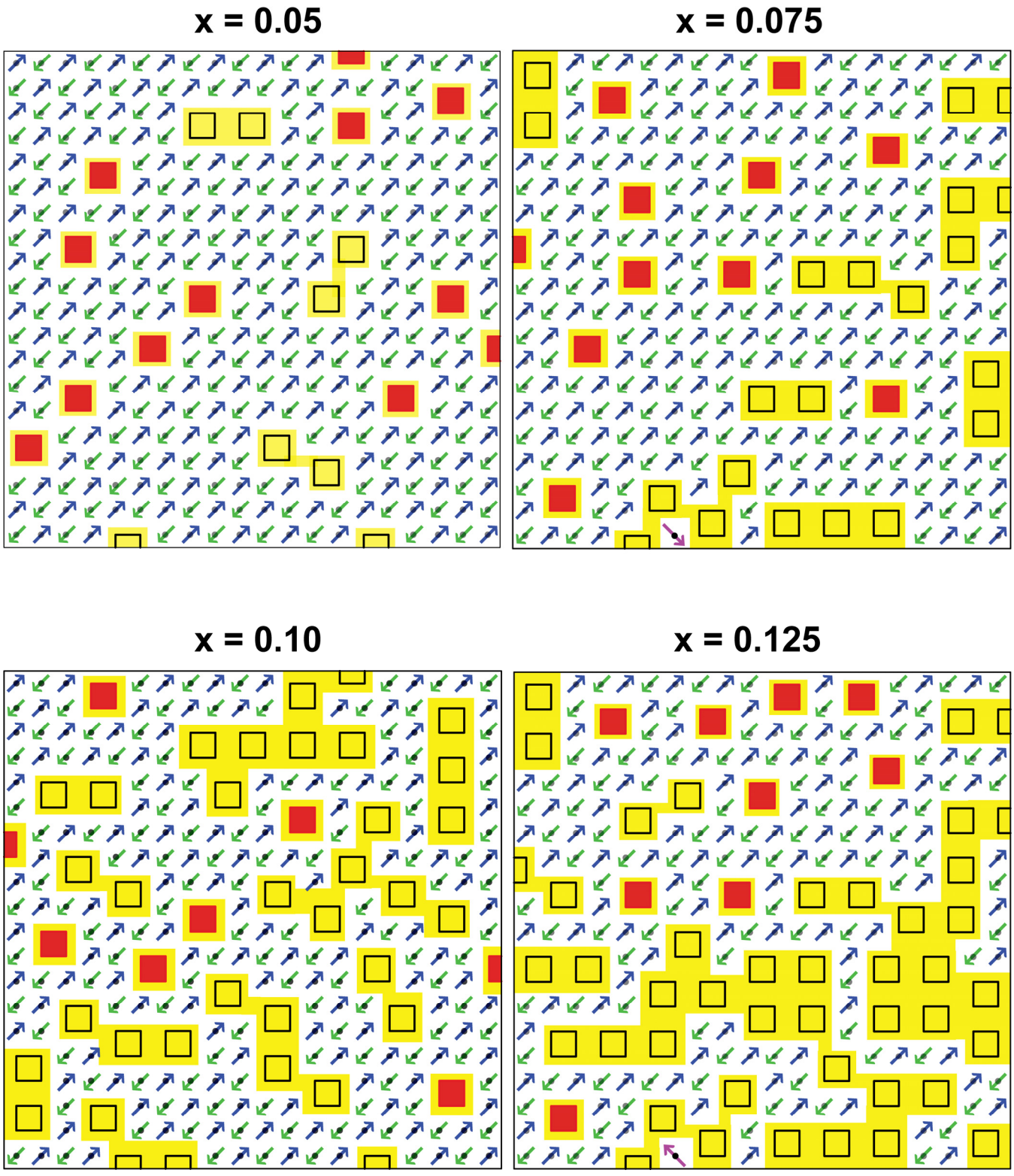

The Figure caption is on page 7

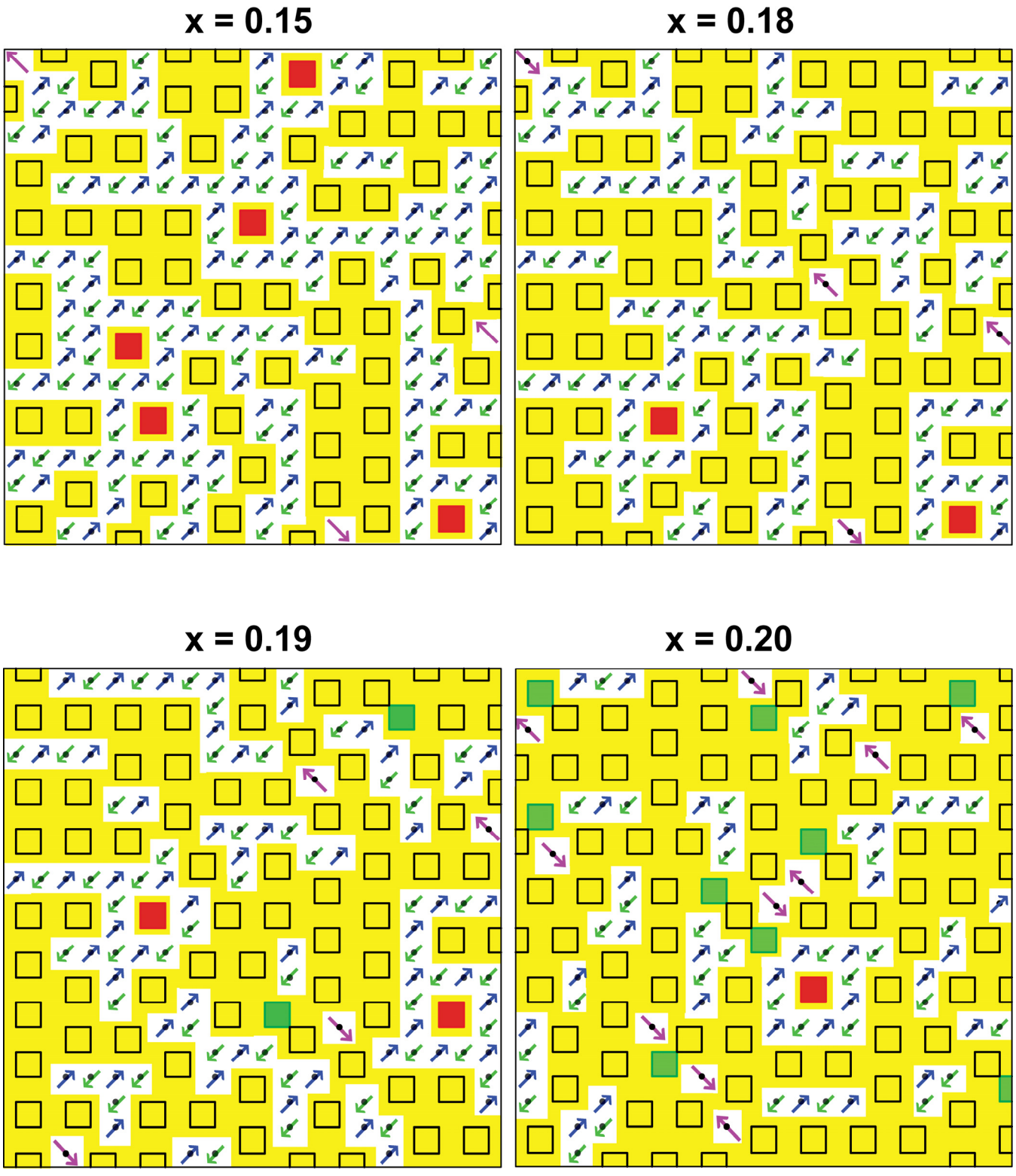

The Figure caption is on page 7

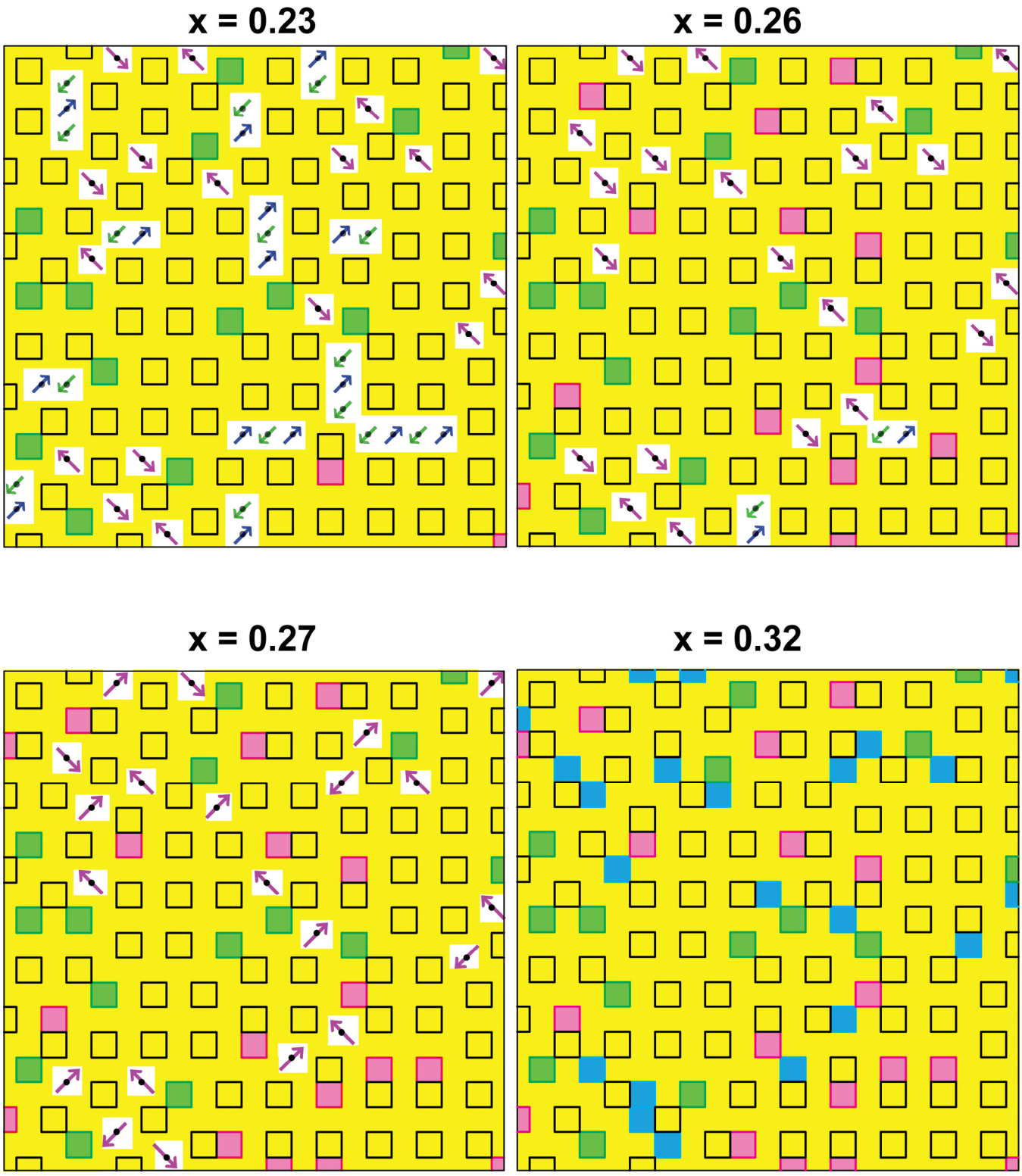

The Figure caption is on page 7

Approximate pinning of P_x and P_y states near Fermi level

The eight possible delocalized Cu x2y2/O pσ eigenstates inside an isolated 4-site plaquette are shown in Figure S2. The states are arranged with the highest energy state at the top and the lowest energy state at the bottom. There are two electrons per O pσ and one electron per Cu x2y2 leading to twelve total electrons. This leaves the degenerate P_x and P_y anti-bonding states with two electrons. Expanding the P_x and P_y states as band k-states, we find P_x has the largest overlap with k = (0, π) and P_y with k = (π, 0). These k states are always found to be close to the Fermi level in cuprates. The energies of these isolated plaquettes states will be shifted by the electrostatic potential inside the crystal arising from the rearrangement of charges that occur at equilibrium when the Fermi energy must become constant throughout the crystal. Since the antiferromagnetic d^9 region has a charge density of one electron per Cu and two electrons per O, the charge density inside isolated plaquettes will be approximately the same. This leads to the Fermi level being placed very close to the degenerate anti-bonding P_x and P_y states. The Fermi level is approximately "pinned" near the degeneracy.

Since the anti-bonding Px and Py states have predominantly (π, 0) and (0, π) character, the PG will appear in angle-resolved-photoemission (ARPES) to be largest at these k-vectors.

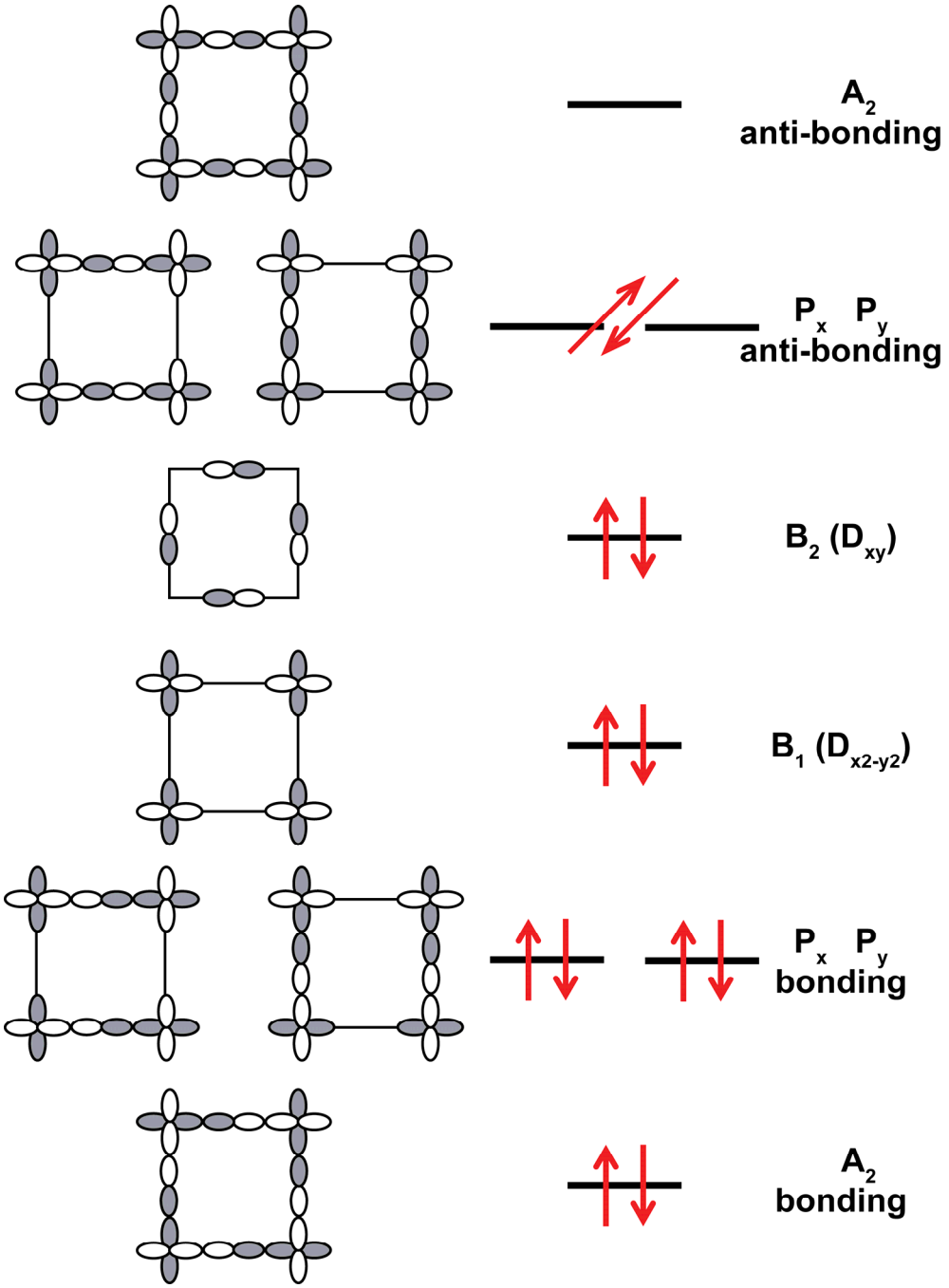

Figure S2 The eight possible delocalized Cu x2y2/O pσ eigenstates inside an isolated 4-site plaquette. The states are arranged with the highest energy state at the top and the lowest energy state at the bottom. There are two electrons per O pσ and one electron per Cu x2y2 leading to twelve total electrons. There are only two electrons to occupy the four degenerate P_x and P_y anti-bonding states. Theses states have dominant k-vector character at $(\pi, 0)$ and $(0, \pi)$, respectively. The splitting of the P_x and P_y states leads to the PG.

Discussion of the diagonal and off-diagonal terms in the 2 x 2 Hamilton matrix for the PG of a particular isolated 4-site plaquette

For a given isolated plaquette located at position **R**, the Hamiltonian matrix for the P_x and P_y orbitals is $H_0 \approx \begin{bmatrix} \varepsilon_F & 0 \\ 0 & \varepsilon_F \end{bmatrix}$, where ε_F is the Fermi energy. The perturbing matrix for coupling of this plaquette to the antiferromagnetic d^9 spins, the delocalized Cu x2y2/O pσ swath, and other isolated plaquettes is $H' \approx \begin{bmatrix} \varepsilon_{xx} & t_{xy}(R) \\ t_{xy}(R) & \varepsilon_{yy} \end{bmatrix}$. We expect the diagonal terms to be approximately the same, $\varepsilon_{xx} \approx \varepsilon_{yy}$, due to the random doping environment. Any non-zero value leads to a particle-hole asymmetry of the PG as is observed.[25,26] Thus the modulus of the off-diagonal term, $|t_{xy}|$, determines the size of the splitting and the PG for this isolated plaquette.

The first expectation is that the dominant coupling of the P_x state to P_y is by second-order coupling through the antiferromagnetic spins neighboring the plaquette. Since the plaquette is isolated, it is completely surrounded by antiferromagnetic spins in the plane and the approximate D_4 symmetry of the plaquette is maintained by including these antiferromagnetic spins. Thus coupling to the antiferromagnetic spins cannot split the degeneracy of the P_x and P_y states.

Coupling of P_x and P_y can occur by interaction through the antiferromagnetic d^9 spins to the delocalized metallic Cu x2y2/O pσ states in the percolating plaquette swath. Since the bandwidth of the metallic band inside the percolating swath is ≈ 2.0 eV and the shape of the metallic swath is random, this coupling should be small.

The largest coupling between P_x and P_y inside a particular isolated plaquette is with states close in energy to P_x and P_y (since the energy difference appears in the denominator in a second-order perturbation). This leads to the dominant coupling through other isolated plaquettes. For two isolated plaquettes to interact, they must couple through the antiferromagnetic d^9 spins. Due to the finite correlation length of the antiferromagnetic spins, ξ, this coupling will be exponentially attenuated for

distances larger than ξ. Thus the magnitude of the PG is a function of the distances between isolated clusters as a function of doping as shown in Figure 3b.

The off-diagonal coupling matrix element, $t_{xy}(\mathbf{R_i})$, where $\mathbf{R_i}$ is the position of the i^{th} isolated plaquette, is the sum of terms, $t_{xy}(\mathbf{R_i}, \mathbf{R_j})$, where $\mathbf{R_j}$ is the position of the j^{th} isolated plaquette

$$t_{xy}(R_i, R_j) = \Delta_0 e^{-|R_i - R_j|/\xi} e^{i\varphi(R_i, R_j)}$$

$$t_{xy}(R_i) = \sum_j t_{xy}(R_i, R_j)$$

The first term in $t_{xy}(\mathbf{R_i}, \mathbf{R_j})$ is the constant, Δ_0. It sets the energy scale of the coupling and should be on the order of the antiferromagnetic spin-spin coupling, J_{dd} = 130 meV. The first exponential is the damping of the matrix element due to transmission through the d^9 antiferromagnetic region with finite correlation length, ξ. The ratio of the distance between the plaquettes, $|\mathbf{R_i} - \mathbf{R_j}|$, and the correlation length determines the magnitude of the damping. The final term is the phase.

Due to the arbitrary distribution of the plaquettes and the antiferromagnetic d^9 environment, we take the phases coupling isolated plaquettes at $\mathbf{R_j}$ and $\mathbf{R_k}$ to the isolated plaquette at $\mathbf{R_i}$ to be uncorrelated, $\langle \varphi(R_i, R_j)\varphi(R_i, R_k) \rangle = 0$, for $j \neq k$.

The PG is given by one-half of the splitting of the P_x and P_y levels, $\Delta_{PG}(R_i) = |t_{xy}(R_i)|$. Due to the random phases, $\varphi(R_i, R_j)$, the PG is the average, $\Delta_{PG}(R_i) = \langle |t_{xy}(R_i)| \rangle$. The average of the modulus can be well approximated by the square root of the average of the modulus squared, leading to

$$\Delta_{PG}(R_i) = \sqrt{\langle |t_{xy}(R_i)|^2 \rangle}$$

$$\Delta_{PG}(R_i) = \Delta_0 \left(\sum_j e^{-2|R_i - R_j|/\xi} \right)^{\frac{1}{2}} \qquad (1)$$

Neutron spin scattering experiments find the correlation length to be approximately equal to the mean spacing of holes, $\xi \approx a/\sqrt{x}$, where a is the nearest-neighbor Cu-Cu distance (a ≈ 3.8 Å) and x is the doping.[27] The above expression is used to compute the PG curve shown in the main text.

An analytic expression for the PG

An approximate analytic expression for Δ_{PG} can be obtained from the computed number of isolated plaquettes as a function of doping, N_4. Due to the exponential decay of the matrix element with length scale, ξ, only isolated plaquettes inside an area on the order of $\sim \xi^2$ can contribute to the sum in Equation 1. Let a be the Cu-Cu distance in the plane and N equal the total number of Cu sites in the plane. Then the average number of isolated plaquettes in the area A is $A\left(\frac{N_4}{Na^2}\right)$. Substituting $A = \xi^2$ leads to the approximate analytic expression

$$\Delta_{PG} = \Delta_0' \sqrt{\frac{N_4 \xi^2}{Na^2}} = \Delta_0' \sqrt{\frac{N_4}{Nx}}$$

Δ_0' is a constant close to Δ_0. Figure S3 shows the fit to the analytic expression above. The fit is quite good, but the exact evaluation of Equation 1 leads to a better fit.

Inhomogeneous PG determination

Equation 1 leads to a different value for the PG for each isolated plaquettes. STM measurements observed an inhomogeneous distribution of the PG with an approximately doping independent standard deviation of ~ 10 – 20 meV. Our calculations also find an approximately constant value of ~ 15 meV.

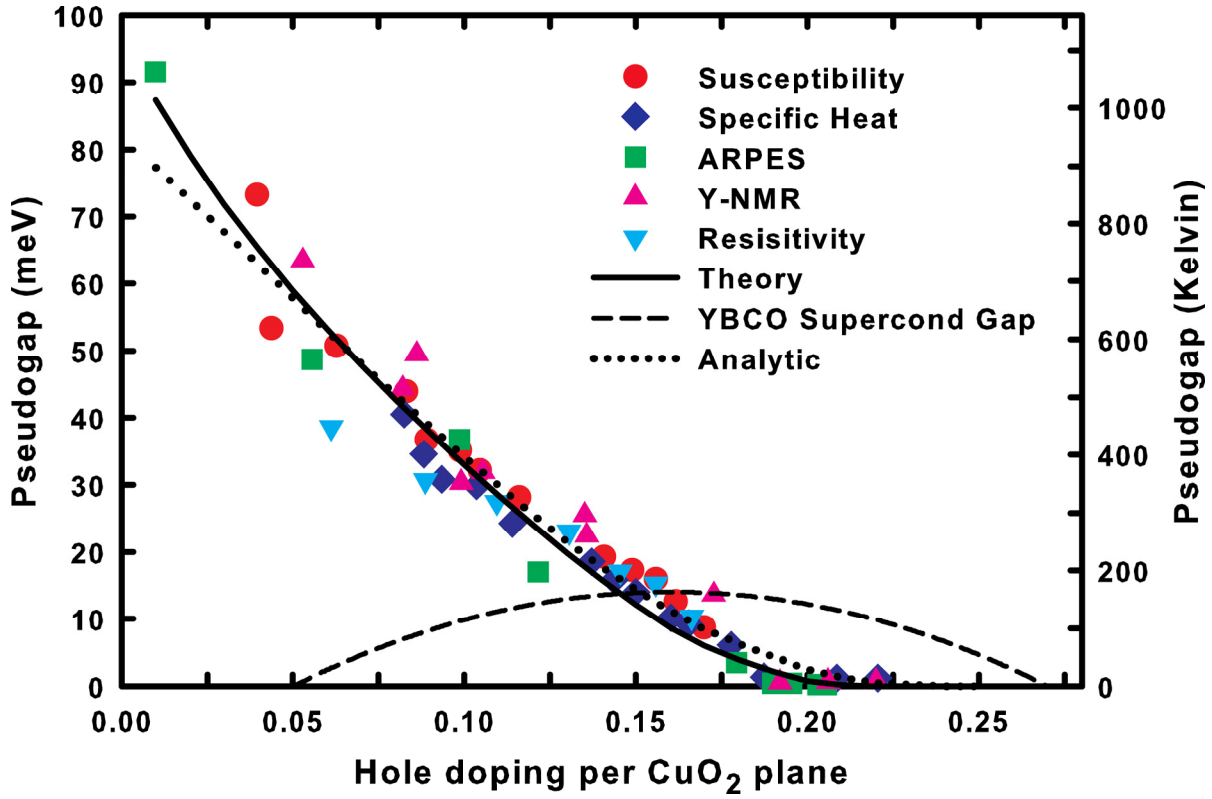

Figure S3. Comparison of calculated PG curve using Equation 1 and the approximate analytic expression, $\Delta_{PG} = \Delta_0' \sqrt{N_4/Nx}$, where $\Delta_0' = 82.4$ meV. Here, N_4 is the total number of isolated plaquettes at doping, x. N is the total number of Cu atoms. The dotted curve is the analytic expression and the solid black curve is calculated from Equation 1. The dashed curve is the superconducting gap, Δ, for $YBa_2Cu_3O_{7-\delta}$ where we use $2\Delta/kT_c = 3.5$ and obtain T_c using the approximate equation,[28] $\left(T_c/T_{c,\max}\right) = 1 - 82.6(x - 0.16)^2$, where $T_{c,max} = 93$ K. The PG from the analytic expression remains non-zero for slightly higher dopings than 0.20 and does not obtain as large of a PG for low doping as the computed result from Equation 1. The data points in the figure are taken from Tallon et al.[29]

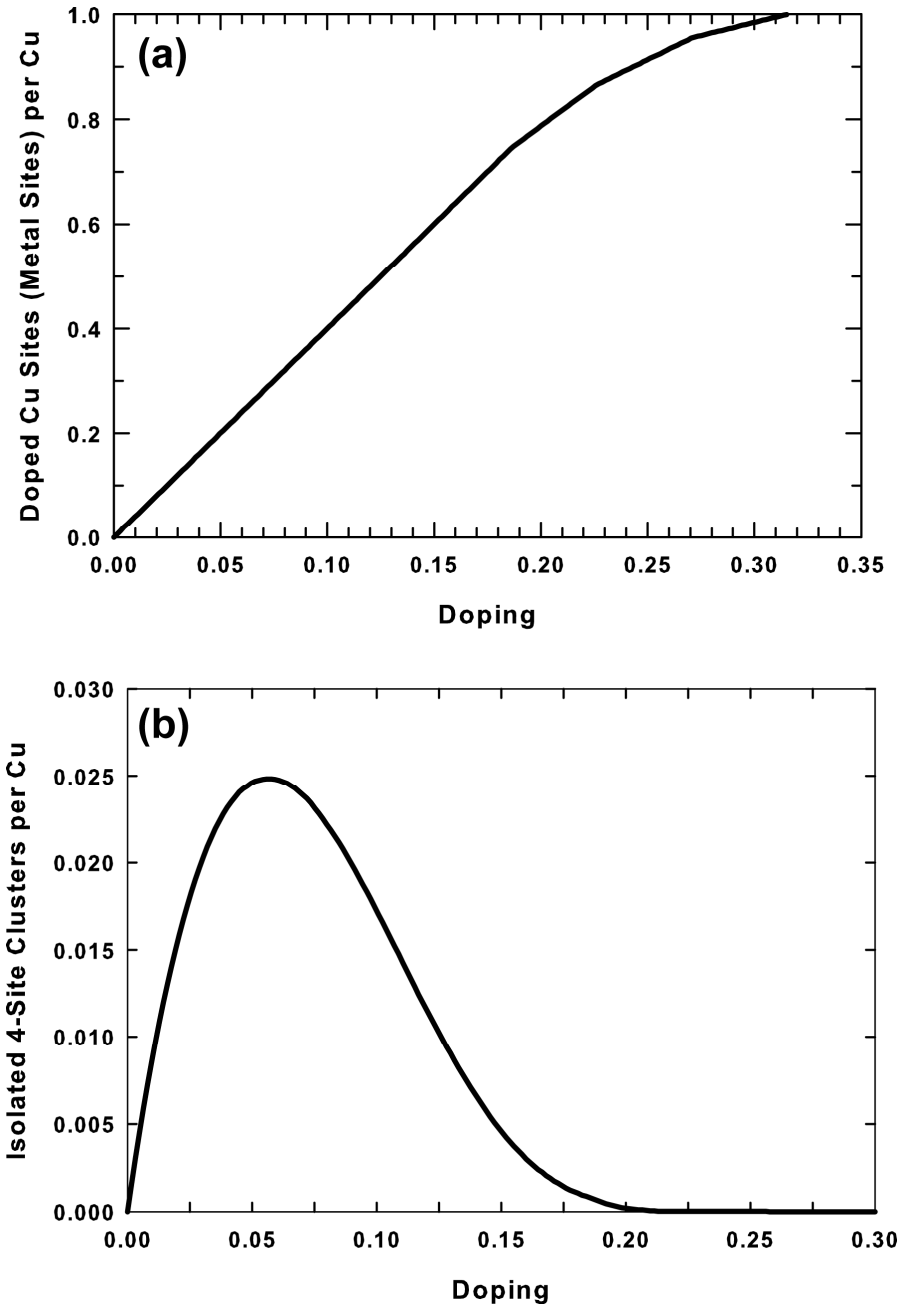

Figure S4. The evolution of the metal sites and isolated plaquettes with doping. In (a), the number of doped Cu sites per total Cu sites is plotted as a function of doping. Above ≈ 0.05 doping, when the plaquettes percolate through the crystal, a metallic Cu x2y2/O pσ band is formed in the percolating swath. The curve increases as $4x$ up to ≈ 0.187 because each plaquette dopes four Cu sites. Further doping increases the doped Cu sites by $3x$ up to ≈ 0.226, by $2x$ from 0.226 – 0.271, and then by x until 0.317 when all Cu sites become doped (metallic). (b) shows the number of isolated 4-site clusters as a function of doping. For extremely low doping, all plaquettes are isolated and the curve increases as x.

There is a peak at ≈ 0.058. At x ≈ 0.20, the number of isolated plaquettes becomes almost zero and the PG vanishes.

References

(1) Newman, M. E. J.; Ziff, R. M. Fast Monte Carlo Algorithm for Site or Bond Percolation. *Phys Rev E.* **2001**, *6401*, 016706.

(2) Yu, J. J.; Freeman, A. J.; Xu, J. H. Electronically Driven Instabilities and Superconductivity in the Layered $La_{2-X}Ba_xCuO_4$ Perovskites. *Phys Rev Lett.* **1987**, *58*, 1035-1037.

(3) Mattheiss, L. F. Electronic Band Properties and Superconductivity in $La_{2-Y}X_yCuO_4$. *Phys Rev Lett.* **1987**, *58*, 1028-1030.

(4) Pickett, W. E. Electronic-Structure of the High-Temperature Oxide Superconductors. *Rev Mod Phys.* **1989**, *61*, 433-512.

(5) Perry, J. K.; Tahir-Kheli, J.; Goddard, W. A. (unpublished). **2001**.

(6) Perdew, J. P.; Levy, M. Physical Content of the Exact Kohn-Sham Orbital Energies - Band-Gaps and Derivative Discontinuities. *Phys Rev Lett.* **1983**, *51*, 1884-1887.

(7) Sham, L. J.; Schluter, M. Density-Functional Theory of the Energy-Gap. *Phys Rev Lett.* **1983**, *51*, 1888-1891.

(8) Perdew, J. P.; Zunger, A. Self-Interaction Correction to Density-Functional Approximations for Many-Electron Systems. *Phys Rev B.* **1981**, *23*, 5048-5079.

(9) Svane, A. Electronic-Structure of La_2CuO_4 in the Self-Interaction-Corrected Density Functional Formalism. *Phys Rev Lett.* **1992**, *68*, 1900-1903.

(10) Temmerman, W. M.; Szotek, Z.; Winter, H. Self-Interaction-Corrected Electronic-Structure of La_2CuO_4. *Phys Rev B.* **1993**, *47*, 11533-11536.

(11) Czyzyk, M. T.; Sawatzky, G. A. Local-Density Functional and on-Site Correlations - the Electronic-Structure of La_2CuO_4 and $LaCuO_3$. *Phys Rev B.* **1994**, *49*, 14211-14228.

(12) Perry, J. K.; Tahir-Kheli, J.; Goddard, W. A. Antiferromagnetic Band Structure of La_2CuO_4: Becke-3-Lee-Yang-Parr Calculations. *Phys Rev B.* **2001**, *63*, 144510.

(13) Perry, J. K.; Tahir-Kheli, J.; Goddard, W. A. Ab Initio Evidence for the Formation of Impurity d_{3z2-r2} Holes in Doped $La_{2-x}Sr_xCuO_4$. *Phys Rev B.* **2002**, *65*, 144501.

(14) Xu, X.; Goddard, W. A. The X3LYP Extended Density Functional for Accurate Descriptions of Nonbond Interactions, Spin States, and Thermochemical Properties. *P Natl Acad Sci USA.* **2004**, *101*, 2673-2677.

(15) Bryantsev, V. S.; Diallo, M. S.; van Duin, A. C. T.; Goddard, W. A. Evaluation of B3LYP, X3LYP, and M06-Class Density Functionals for Predicting the Binding Energies of Neutral, Protonated, and Deprotonated Water Clusters. *J Chem Theory Comput.* **2009**, *5*, 1016-1026.

(16) Curtiss, L. A.; Raghavachari, K.; Trucks, G. W.; Pople, J. A. Gaussian-2 Theory for Molecular-Energies of 1st-Row and 2nd-Row Compounds. *J Chem Phys.* **1991**, *94*, 7221-7230.

(17) Curtiss, L. A.; Raghavachari, K.; Redfern, P. C.; Pople, J. A. Assessment of Gaussian-2 and Density Functional Theories for the Computation of Enthalpies of Formation. *J Chem Phys.* **1997**, *106*, 1063-1079.

(18) Matsuda, Y.; Tahir-Kheli, J.; Goddard, W. A. Definitive Band Gaps for Single-Wall Carbon Nanotubes. *J Phys Chem Lett.* **2010**, *1*, 2946-2950.

(19) Xiao, H.; Tahir-Kheli, J.; Goddard, W. A. Accurate Band Gaps for Semiconductors from Density Functional Theory. *J Phys Chem Lett.* **2011**, *2*, 212-217.

(20) Mori-Sanchez, P.; Cohen, A. J.; Yang, W. T. Localization and Delocalization Errors in Density Functional Theory and Implications for Band-Gap Prediction. *Phys Rev Lett.* **2008**, *100*, 146401.

(21) Haskel, D.; Stern, E. A.; Hinks, D. G.; Mitchell, A. W.; Jorgensen, J. D. Altered Sr Environment in $La_{2-x}Sr_xCuO_4$. *Phys Rev B.* **1997**, *56*, R521-R524.
(22) Tahir-Kheli, J.; Goddard, W. A. Chiral Plaquette Polaron Theory of Cuprate Superconductivity. *Phys Rev B.* **2007**, *76*, 014514.
(23) Tahir-Kheli, J.; Goddard, W. A. The Chiral Plaquette Polaron Paradigm (CPPP) for High Temperature Cuprate Superconductors. *Chem Phys Lett.* **2009**, *472*, 153-165.
(24) Tahir-Kheli, J.; Goddard, W. A. Universal Properties of Cuprate Superconductors: T_c Phase Diagram, Room-Temperature Thermopower, Neutron Spin Resonance, and STM Incommensurability Explained in Terms of Chiral Plaquette Pairing. *J Phys Chem Lett.* **2010**, *1*, 1290-1295.
(25) Hashimoto, M.; He, R. H.; Tanaka, K.; Testaud, J. P.; Meevasana, W.; Moore, R. G.; Lu, D. H.; Yao, H.; Yoshida, Y.; Eisaki, H. et al. Particle-Hole Symmetry Breaking in the Pseudogap State of Bi2201. *Nat Phys.* **2010**, *6*, 414-418.
(26) He, R. H.; Hashimoto, M.; Karapetyan, H.; Koralek, J. D.; Hinton, J. P.; Testaud, J. P.; Nathan, V.; Yoshida, Y.; Yao, H.; Tanaka, K. et al. From a Single-Band Metal to a High-Temperature Superconductor via Two Thermal Phase Transitions. *Science.* **2011**, *331*, 1579-1583.
(27) Kastner, M. A.; Birgeneau, R. J.; Shirane, G.; Endoh, Y. Magnetic, Transport, and Optical Properties of Monolayer Copper Oxides. *Rev Mod Phys.* **1998**, *70*, 897-928.
(28) Presland, M. R.; Tallon, J. L.; Buckley, R. G.; Liu, R. S.; Flower, N. E. General Trends in Oxygen Stoichiometry Effects on T_c in Bi and Tl Superconductors. *Physica C.* **1991**, *176*, 95-105.
(29) Tallon, J. L.; Loram, J. W. The Doping Dependence of T* - What is the Real high-T_c Phase Diagram? *Physica C.* **2001**, *349*, 53-68.